International Journal of Precision Engineering and Manufacturing (2020) 21:1–9
https://doi.org/10.1007/s12541-019-00232-8

Online ISSN 2005-4602
Print ISSN 2234-7593

REGULAR PAPER

Single-Point Grinding of Alumina and Zirconia Ceramics Under Two-Dimensional Compressive Prestress

Gaofeng Zhang[1] · Zhigang Wang[2] · Wenxin Chen[2] · Jingtao Li[2] · Hao Sun[2] · Kui Zhang[2]

Received: 5 August 2018 / Revised: 8 July 2019 / Accepted: 4 September 2019 / Published online: 23 October 2019

Abstract
In this study, single-point grinding experiments were performed on alumina and zirconia ceramics to investigate the grinding processes under two-dimensional compressive prestress (TCP). Grinding forces and grooves were measured under different values of TCP to evaluate the grinding defects. The material removal rate and actual grinding depth were exploited to investigate the grinding-induced damage and material removal mechanisms. The results demonstrate that the grinding forces show an increasing tendency with the increasing values of TCP, while the cracks and chipping along the grinding groove edges of both alumina and zirconia ceramics can be reduced. In addition, the material removal rates of both alumina and zirconia ceramics show the same change tendency with the grinding-induced damage for decreasing the actual grinding depth under different values of TCP.

Keywords Alumina and zirconia ceramics · Grinding induced-damage · Prestress · Principal stress

Abbreviation
TCP two-dimensional compressive prestress

1 Introduction

Owing to the advantages, such as good wear resistance, high thermal stability, and excellent corrosion resistance, engineering ceramics have been widely used in industrial applications [1, 2]. However, such ceramics could easily induce machining damage [3] because of their inherent brittleness, leading to unpredictable effects on the reliability and longevity of ceramic parts [4, 5]. Thus, the enhancement of the machining quality and processing efficiency of engineering ceramics has been a key point of the corresponding study, and great efforts have been made towards improving the machining process, especially the grinding process.

The damage mechanisms of engineering ceramics are related to the material removal mode [6], and some novel processing methods have been proposed to investigate these mechanisms. Bifano et al. [7] performed the plunge grinding experiments on fused silica and confirmed that brittle materials would undergo plastic flow instead of fracture when the depth of machining was small enough. Dai et al. [8] also studied the feasibility of ductile machining of hard and brittle materials, and confirmed that when the actual depth of the cut was below the critical value, the material removal pattern changed from brittle to ductile regime machining. Kttagawa and Maekawa [9] proposed a hot-machining technique using plasma jet heating. The machinabilities of Pyrex, mullite, and silicon nitride were greatly improved by hot machining, whereas those of alumina and zirconia ceramics were not. Furthermore, to obtain low force, high quality, and high productivity of brittle materials [10], Ramesh et al. [11] observed the variations of grinding forces and surface quality improvements at velocities of 40–160 m/s in the grinding of SiC as well as alumina and zirconia ceramics.

Manufacturing under compressive prestress is a processing method in which compressive prestress is exerted on a

✉ Gaofeng Zhang
zgfxu@xtu.edu.cn

Zhigang Wang
kg8090@163.com

Wenxin Chen
947578100@qq.com

Jingtao Li
819840255@qq.com

Hao Sun
sun_hao6@163.com

Kui Zhang
zhangk@xtu.edu.cn

[1] Engineering Training Center, Xiangtan University, Xiangtan 411105, China

[2] School of Mechanical Engineering, Xiangtan University, Xiangtan 411105, China

workpiece, in which the surface and subsurface damage can be restrained, before its actual manufacture practice. Heard and Cline [12] applied axial pressure on the cylindrical beryllium oxide and aluminum nitride ceramics. On this condition, the fracture mechanism of beryllium oxide ceramic underwent a transition from brittle fracture at low pressure to plastic flow at high pressure. Yet, aluminum-nitride ceramic did not show a similar tendency. Huang et al. [13] numerically simulated a rock-surface indentation process with respect to lateral stress, and noted that the lateral stress played a significant role in the crack extension in rock. Considering that a hydrostatic condition can constrain the deformation in plastic forming processes [14], Yoshino et al. [15, 16] operated single-point cutting and scratching experiments on silicon, quartz, and glass under high hydrostatic pressure. The results indicated that high hydrostatic pressure was required for arresting the process of the crack formation. Besides, scratching experiments were conducted on alumina ceramic [17] and silicon carbide ceramic [18] under conditions of compressive prestress, respectively. The results showed that compressive prestress could effectively suppress damage during scratching.

From researches above, compressive prestress showed a significant influence on constraining induced-damage during manufacture processes. However, very few researches focused on induced-damage during grinding processes. Thus, in this study, single-point grinding experiments were carried out with and without TCP by using a clamp for prestressing to investigate the impact mechanisms of the TCP on the grinding-induced damage of alumina and zirconia ceramics, such as crack, debris, plastic deformation. What's more, a corresponding model was established to explain the stress state after the TCP applied.

2 Experimental Procedure

The study materials are alumina and zirconia ceramics, which are commercially available. The specimens have a dimension of 10 mm × 10 mm × 10 mm. Their mechanical properties at ambient temperature are shown in Table 1.

Compressive prestress was applied using a TCP loading clamp, as shown in Fig. 1. The clamp consists of two V-blocks, a high-strength pressure bolt, a nut, a strain-gauge pressure sensor, and a display device. Figure 2 was the diagram of the single-point grinding process. The lateral loading force was exerted by rotating the high-strength pressure bolt, from which signal acquisition was collected by the sensor, amplified using an amplifier, and displayed on the display device. Single-point grinding experiments were conducted on MGK7120X60/1 high-precision grinding machine with a self-designed single-point grinding wheel, as shown in Fig. 3. The tip of the cutting tool was a diamond grain. Table 2 lists the experimental grinding parameters.

Table 1 Properties of alumina and zirconia ceramics

Mechanical properties	Alumina	Zirconia
Density (kg/m$^{3)}$	3.7	6.1
Elastic modulus (GPa)	300	210
Compressive strength (MPa)	2500	2000
Poisson's ratio	0.2	0.3
Hardness (GPa)	17.5	11.8
K_{IC} (MPa/m$^{1/2}$)	3.5	10

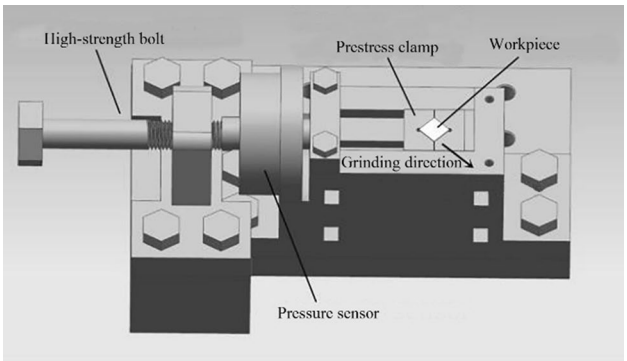

Fig. 1 TCP loading clamp

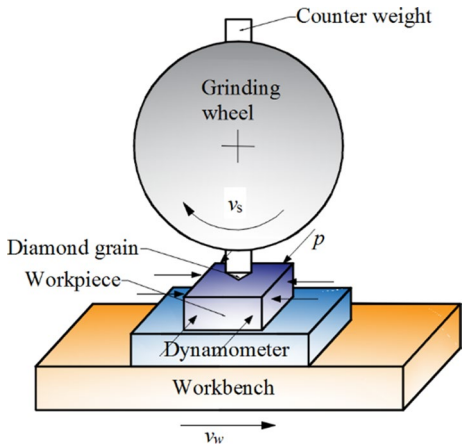

Fig. 2 The diagram of the single-point grinding process

For the experiments, the grinding depth was set at 5, 10, and 20 μm. During the experiments, grinding forces were measured using a dynamometer (Kistler 9257B). After grinding, the specimens were cleaned with acetone in an ultrasonic cleaner. The 3-dimensional profiles of grinding grooves were scanned using the Keyence VHX-2000 microscope, which was also used to measure the material removal volume. After conductive coating, the morphologies of grinding grooves were observed through the JSM-6360 scanning electron microscope.

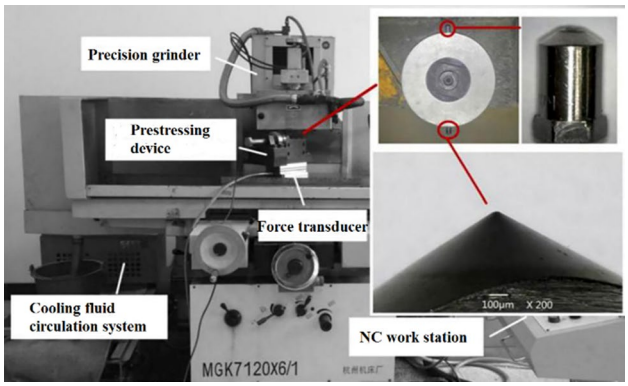

Fig. 3 Manufacture device for machining test with two-dimensional compressive prestress

Table 2 Conditions of grinding experiments

Grinding parameter	Value
Wheel speed (m/s)	22.8
Table speed (m/min)	1
Grinding depth (μm)	5, 10, 20
Environmental conditions	Atmospheric
Coolant	None

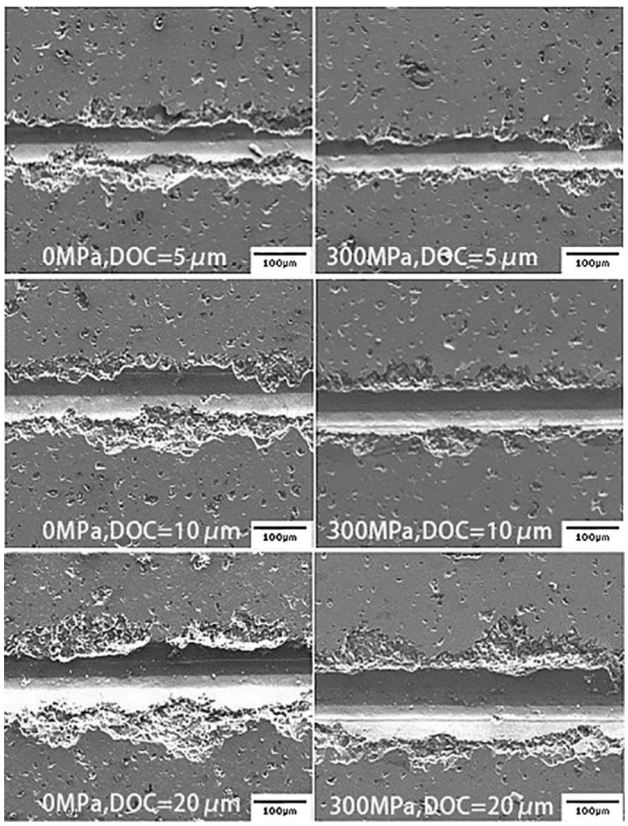

Fig. 4 Micrographs of grinding grooves of alumina

3 Results

3.1 Surface Morphology

The features of typical grinding grooves of alumina ceramic are shown in Fig. 4. The micrographs reveal the grinding induced-damage and severe chipping along the groove edges of the alumina ceramic. The chipping scale increased with the increase of grinding depth. In addition, the chipping and fracture were so severe that the groove edge almost could not be observed under the condition of 0 MPa when grinding depths were 10 and 20 μm. Nevertheless, the chipping region of alumina ground under 300 MPa TCP is smaller than that under 0 MPa. The severe chipping resulted from the expansion of grinding-induced damage, while the cracks intersected with each other and possibly connected to pores, eventually leading to chipping. Figure 5 shows the magnified grinding grooves. For the sample's surface ground under 0 MPa TCP, cracks were seen passing through the center of the groove; however, these cracks were observed less frequently on the sample's surface ground under 300 MPa TCP. The surface of the grinding track contained parallel micro cracks perpendicular to the grinding direction. In addition, debris was seen on the grinding track, and the substrate material underwent plastic deformation.

Figure 6 presents micrographs of the grinding grooves of zirconia ceramic. Unlike the alumina ceramic, the grooves are relatively smooth with a straight edge. Occasional chipping and cracks can be observed along the groove edges. In general, less chipping occurs on the groove surface ground under 300 MPa TCP than that under 0 MPa. Further examination under higher magnification revealed more details of the grinding track, as shown in Fig. 7. The grooves present plastic deformation characteristics for both conditions; however, the grinding track surface under 300 MPa TCP is neater and smoother than that under 0 MPa. There remains debris that has undergone plastic deformation on the bottom of the groove surface under 0 MPa TCP. Pits can be observed on the grinding tracks on both samples' surfaces under 0 and 300 MPa TCP.

3.2 Material Removal Volume

Figure 8 shows typical 3-dimensional profiles of grinding grooves and cross-section profiles of alumina ceramic at the grinding depth of 20 μm, scanned through the Keyence VHX-2000. The comparison of Fig. 8a with Fig. 8b shows that under the condition of TCP, either the practical grinding depth or groove width of alumina ceramic decreases. To elucidate them, the volume of the material removed was calculated using the Keyence VHX-2000 according to the groove profile. Figure 9 provides a comparison of material removal rates of alumina and zirconia ceramics when grinding and

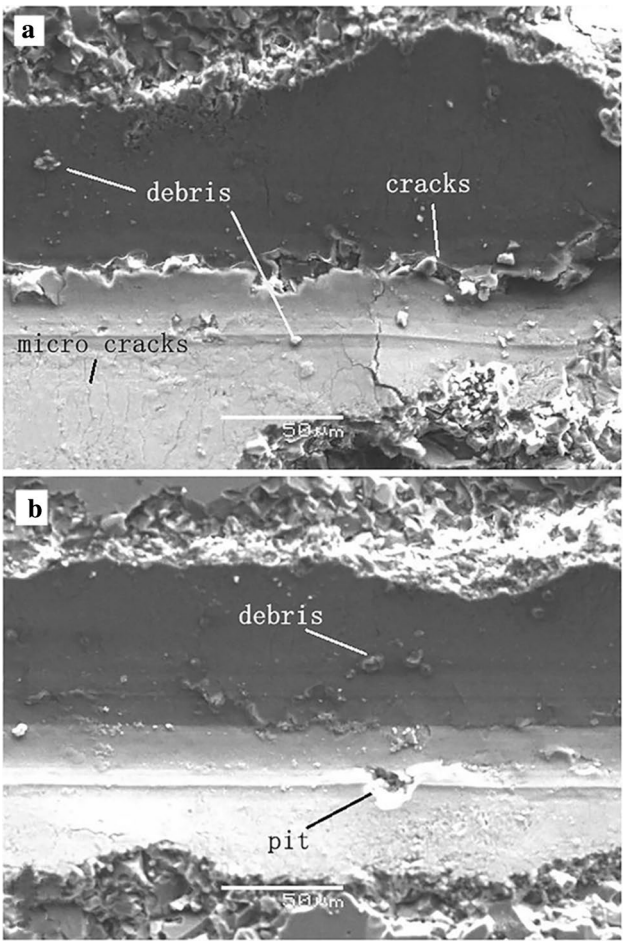

Fig. 5 Micrographs of grinding grooves of alumina ground at 20 μm depth under TCP of **a** 0 MPa and **b** 300 MPa

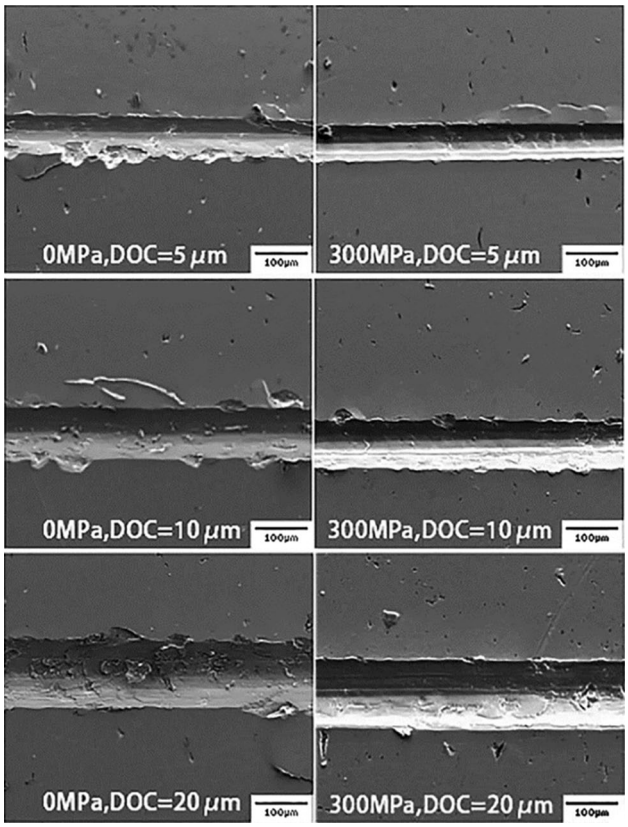

Fig. 6 Micrographs of grinding grooves of zirconia

not grinding under TCP. As shown, the existence of TCP results in lower material removal rates; this could partially be due to the existence of TCP results in the lower actual grinding depths of both alumina and zirconia ceramics. In addition, the reduction in chipping and fragments also results in smaller material removal rate when TCP is applied. This can be explained by the fact that the compressive prestress reduces the actual grinding depth and inhibits cracks, including lateral cracks that extend to free surface and make the material removed. Eventually the material removal volume decreases. As shown in Fig. 10, for the machine stiffness [19], the actual grinding depth is lower than the setting grinding value, and the TCP also diminishes the actual grinding depth. But with the grinding depth increases, the ratios of both alumina and zirconia ceramics become smaller.

3.3 Grinding Force

During material grinding processes, ductile deformation, chip forming and friction between the grinding wheel and workpiece are related to the grinding forces. In this study, the normal grinding force was measured during the grinding processes of both alumina and zirconia ceramics. The values of average normal forces are plotted in Fig. 11. Notably, the normal grinding forces of both materials increase with the increase in grinding depth and TCP values. This phenomenon can be interpreted by the emergence of a corresponding stress to result in higher grinding forces for both alumina and zirconia ceramics when the TCP is applied. For alumina ceramic, compressive prestress has a scarce influence on the grinding force when the grinding depth is 5 μm, yet slightly increases the grinding force when the grinding depth increases. Further, for zirconia ceramic, normal grinding force tends to significantly increase under 300 MPa TCP compared with alumina ceramic when the grinding depth is 5 μm. According to surface topography, the increasing grinding force will not intensify the grinding-induced damage but could shorten the longevity of the grinding wheel.

3.4 Discussion

Chipping and cracks occurred under both conditions of the grinding processes of alumina and zirconia ceramics. The origins of machining defects are not present on or near

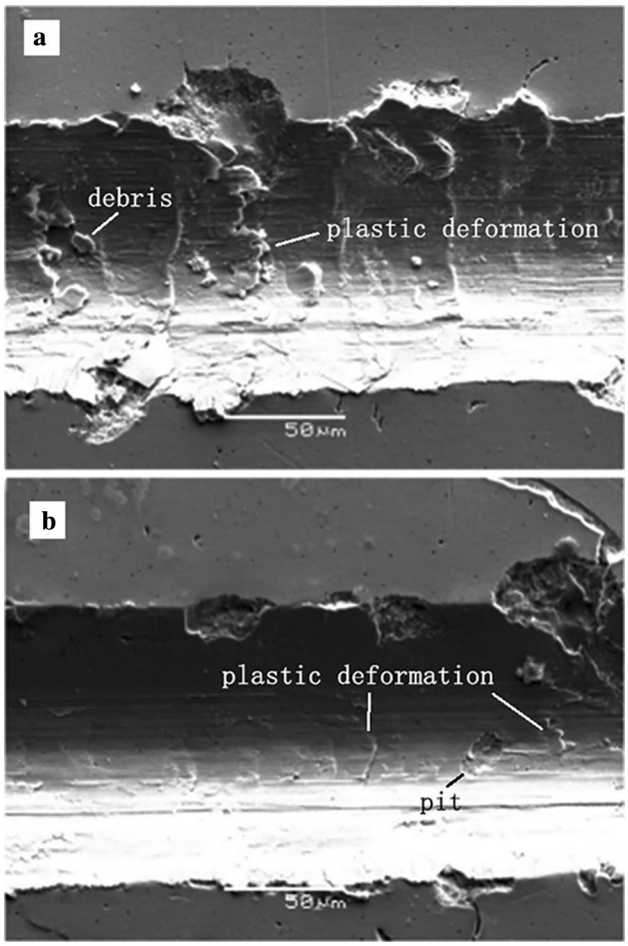

Fig. 7 Micrographs of grinding grooves of zirconia ground at 20 μm depth under TCP of **a** 0 MPa and **b** 300 MPa

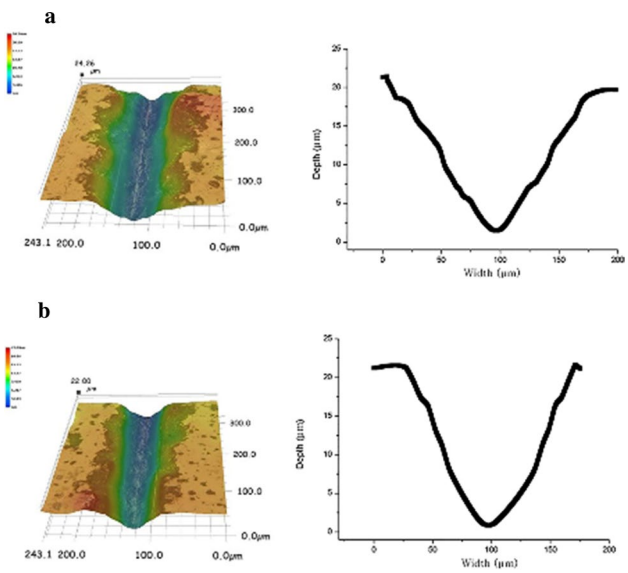

Fig. 8 Typical 3-dimensional profiles of grinding grooves and cross-section profiles of alumina at **a** 0 MPa and **b** 300 MPa

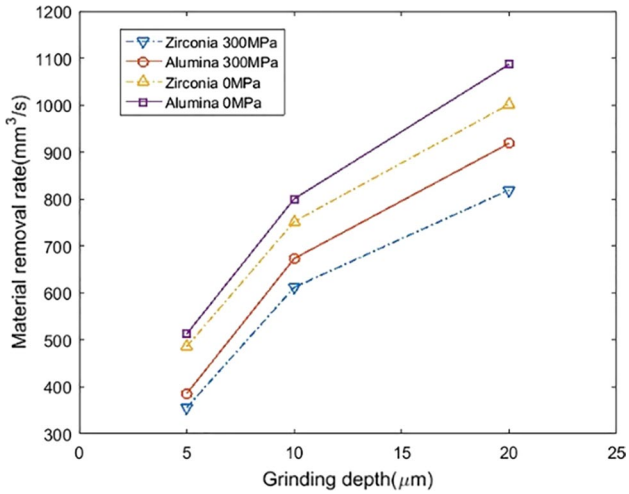

Fig. 9 Material removal rates of alumina and zirconia

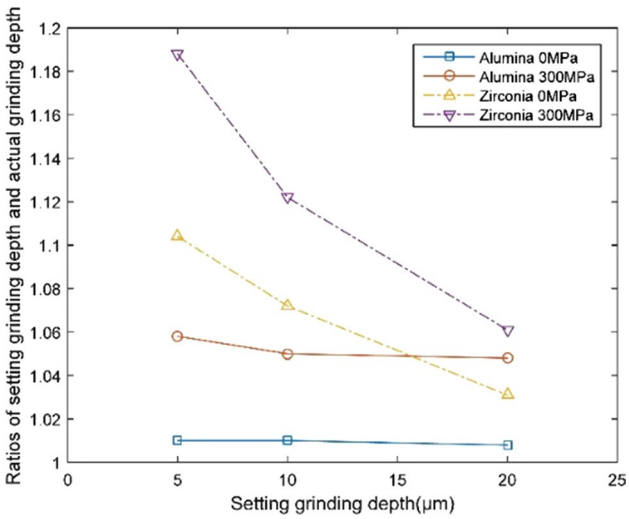

Fig. 10 The effect of prestress on grinding depth ratios

the surface but in the interior of the specimen [16]. For the machining defects that originated inside the specimen, the prestress can prevent crack propagation by balancing the stress that induces the crack and chipping. This agree well with the observation of grinding grooves indicating that compressive prestress reduces the chipping and cracks (Figs. 4 and 6).

Figure 12 showed the coordinate system of the TCP grinding process. In the previous research [20], stress components had been given, respectively. Besides, Jiang and Tan [21] studied the stress field during the single-point scratching process. Based on the researches above, establishing the Boussinesq potential function, the stress state of a certain point in the cylindrical coordinate system was given as Eq. (1).

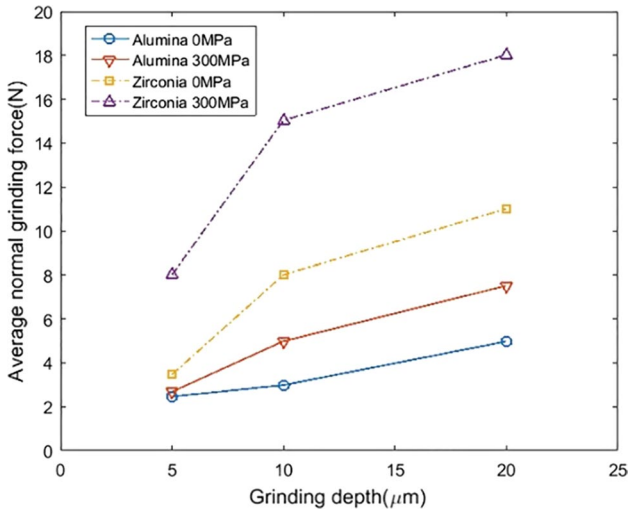

Fig. 11 Average normal grinding force of ceramics

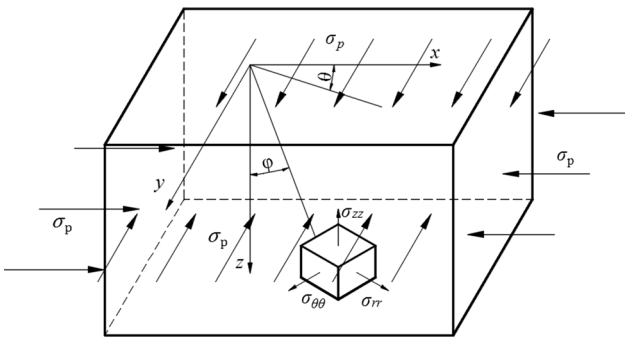

Fig. 12 Coordinate system of the TCP grinding process

material under the compressive prestress. When λ is close to the friction coefficient of the material and scriber (e.g., $0<\lambda<1$), it can be characterized for the scratching process. When λ is large (e.g., $\lambda>1$), it can be used to describe the grinding process of the single-diamond grain under compressive prestress.

As the previous research confirmed [22], tensile stresses are likely to cause crack initiation and propagation, while shear stresses induce surface chipping. When $\theta = 0$, the principle stresses reach their extreme values, the $\sigma_{r\theta} = \sigma_{z\theta} = 0$. Hence, to elucidate the machining mechanism of engineering ceramics, the principle stress field can be a key factor. The stress state expressed by Eq. (1) can be transformed into the principal stress field, consisting of principal stresses σ_1, σ_2, and σ_3, given as Eq. (2) [23].

$$\begin{aligned}\sigma_1 &= \frac{\sigma_{rr}+\sigma_{zz}}{2} + \sqrt{\left(\frac{\sigma_{rr}-\sigma_{zz}}{2}\right)^2 + \sigma_{rz}^2}\\ \sigma_2 &= \sigma_{\theta\theta}\\ \sigma_3 &= \frac{\sigma_{rr}+\sigma_{zz}}{2} - \sqrt{\left(\frac{\sigma_{rr}-\sigma_{zz}}{2}\right)^2 + \sigma_{rz}^2}\end{aligned} \tag{2}$$

Usually, the principal stresses are arranged in the sequence of their algebraic values. The first principal stress σ_1, if positive, is the maximum tensile stress. According to the principal stress, the maximum shear stress is given as follows:

$$\tau_{max} = \frac{\sigma_1 - \sigma_3}{2} \tag{3}$$

The maximum stress is supposed to occur in the plane just underneath the abrasive grain [22], that is the plane with $\theta=0$; thus, we discuss stress distribution in this plane. The

$$\begin{aligned}\sigma_{rr} &= \frac{F_Z}{2\pi R^2}\left(\frac{1-2\nu}{1+cos\varphi} - 3sin^2\varphi cos\varphi\right) + \frac{F_Z\lambda cos\theta}{2\pi R^2}\left(\frac{(1-2\nu)sin\varphi}{(1+cos\varphi)^2} - 3sin^3\varphi\right) - \sigma_p\\ \sigma_{\theta\theta} &= \frac{F_Z(1-2\nu)}{2\pi R^2}\left(cos\varphi - \frac{1}{1+cos\varphi}\right) + \frac{F_Z(1-2\nu)\lambda cos\theta sin\varphi}{2\pi R^2}\left(1 - \frac{1}{(1+cos\varphi)^2}\right) - \sigma_p\\ \sigma_{zz} &= -\frac{3F_Z}{2\pi R^2}cos^2\varphi(cos\varphi + \lambda cos\theta sin\varphi)\\ \sigma_{r\theta} &= \frac{F_Z\lambda}{2\pi R^2}sin\theta(1-2\nu)\frac{sin\varphi}{(1+cos\varphi)^2} - 2\sigma_p cos\theta sin\theta\\ \sigma_{rz} &= -\frac{3F_Z}{2\pi R^2}cos\varphi sin\varphi(cos\varphi + \lambda cos\theta sin\varphi)\\ \sigma_{z\theta} &= 0\end{aligned} \tag{1}$$

where σ_{rr}, $\sigma_{\theta\theta}$, and σ_{zz} are normal stress components in the cylindrical coordinate system; σ_p is the compressive prestress; F_z is the normal force; λ is the ratio of normal and tangential forces; R is the distance between the stress unit and origin coordinate. Equation (1) clearly shows that the stress state of a stress unit inside the material is related to the load, Poisson's ratio, position of the unit (θ and φ), and prestress. Note that when $\lambda=0$, the machining mechanics model can be used to describe the indentation process of the

curves of the principal stresses of the single-point grinding mechanic model calculated through Matlab in the plane with $\theta = 0$ are plotted in Fig. 13. The selected parameters are $F_z = 8$ N, $R=60$ μm, $\lambda=1.3$, and $\nu=0.2$. The figure shows that the algebraic values of all three principal stresses decrease with the increase of TCP. From the picture, it is easy to get that σ_1 is always the tensile stress while σ_3 is always the compressive stress when there is no TCP. And σ_2 is a hoop stress. Further, the primary principal stress changes

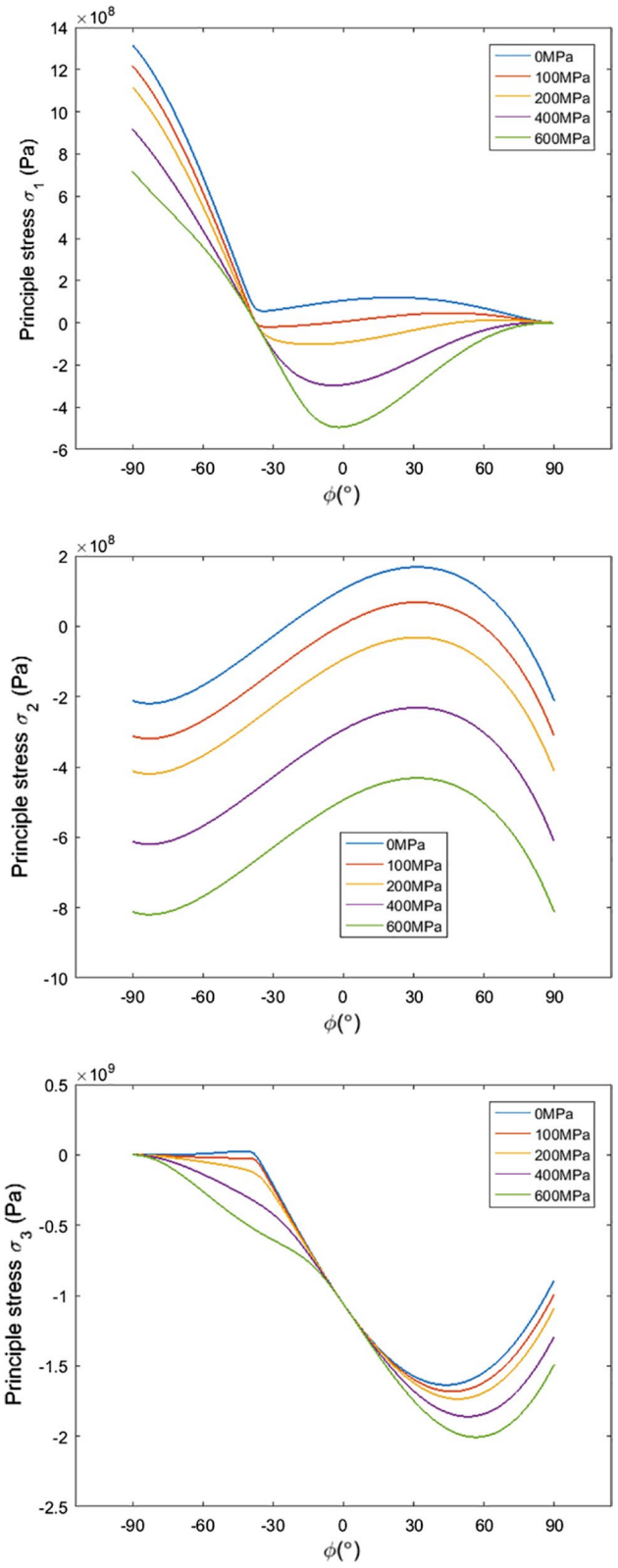

Fig. 13 Principal stresses in the plane with $\theta = 0$

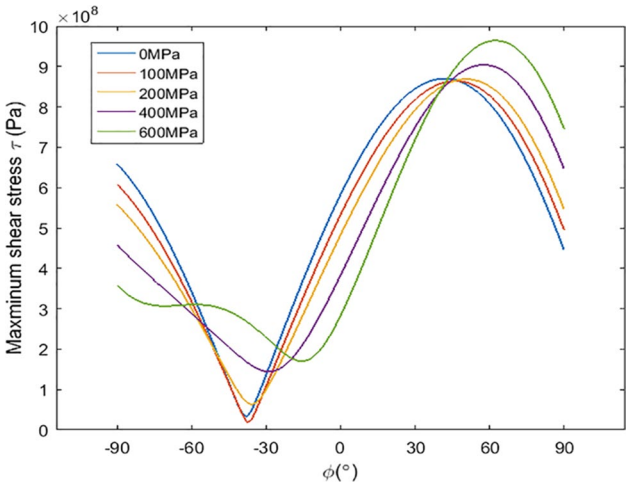

Fig. 14 Maximum shear stress in the plane with $\theta = 0$

from the tensile stress to the compressive stress when the TCP is exerted. And the second and third principal stress are in a situation of the compressive stress. Figure 14 shows that the maximum shear stress reduces in the region around the abrasive grain ($-40° < \varphi < 40°$) when the compressive prestress increases. The reducing of the maximum principle and shear stresses can explain the reduction of chipping and cracks. Furthermore, the reduction of chipping and cracks is in a good agreement with the ground surface characteristics of experimental results (Figs. 4 and 6). However, continuing to increase the value of TCP will lead to deterioration of the ground surface.

4 Conclusion

In this research, single-point grinding experiments were performed on alumina and zirconia ceramics ground and not ground under TCP to investigate the grinding-induced damage. Less amounts of grinding-induced damage, such as cracks and chipping, were observed under an appropriate value of TCP. These phenomena can interpret that origins of machining defects are arrested by the TCP, and the crack propagation and chipping are prevented eventually. In addition, an appropriate value of TCP can reduce the maximum principle and shear stresses so that the propagation of cracks and chipping can be inhibited. While the TCP is applied, either the grinding depths of both alumina and zirconia ceramics decrease or the widths of the grinding grooves decrease, leading to smaller material removal rates. For the action of TCP, corresponding stresses should occur, resulting in higher grinding forces for both alumina and zirconia ceramics.

Acknowledgements The work was supported by the National Natural Science Foundation of China (NSFC) (Project Nos. 51775469, 51704256, 91860133) and Hunan Province Natural Science Foundation (Project No. 2017JJ4051).

References

1. Agarwal, S., & Rao, P. V. (2008). Experimental investigation of surface/subsurface damage formation and material removal mechanisms in SiC grinding. *International Journal of Machine Tools and Manufacture, 48,* 698–710. https://doi.org/10.1016/j.ijmachtools.2007.10.013.
2. Xie, J., Li, Q., Sun, J. X., & Li, Y. H. (2015). Study on ductile-mode mirror grinding of SiC ceramic freeform surface using an elliptical torus-shaped diamond wheel. *Journal of Materials Processing Technology, 222,* 422–433. https://doi.org/10.1016/j.jmatprotec.2015.03.027.
3. Malkin, S., & Ritter, J. E. (1989). Grinding mechanisms and strength degradation for ceramics. *Journal of Engineering for Industry, 111,* 167–174.
4. Zhang, B., Zheng, X. L., Tokura, H., & Yoshikawa, M. (2003). Grinding induced damage in ceramics. *Journal of Materials Processing Technology, 132,* 353–364. https://doi.org/10.1016/S0924-0136(02)00952-4.
5. Lee, S. J., Do, Kim J., & Suh, J. (2014). Microstructural variations and machining characteristics of silicon nitride ceramics from increasing the temperature in laser assisted machining. *International Journal of Precision Engineering and Manufacturing, 15,* 1269–1274. https://doi.org/10.1007/s12541-014-0466-y.
6. Zhang, Q., Fu, Y., Su, H., et al. (2018). Surface damage mechanism of monocrystalline silicon during single point diamond grinding. *Wear, 396–397,* 48–55. https://doi.org/10.1016/j.wear.2017.11.008.
7. Bifano, G. T. (1991). Ductile-regime grinding: A new technology for machining brittle materials. *Journal of Engineering for Industry, 113,* 184.
8. Dai, J., Su, H., Yu, T., et al. (2018). Experimental investigation on materials removal mechanism during grinding silicon carbide ceramics with single diamond grain. *Precision Engineering, 51,* 271–279. https://doi.org/10.1016/j.precisioneng.2017.08.019.
9. Kttagawa, T., & Maekawa, K. (1990). Plasma hot machining for new engineering materials. *Wear, 139,* 251–267. https://doi.org/10.1016/0043-1648(90)90049-G.
10. Huang, H., & Liu, Y. C. (2003). Experimental investigations of machining characteristics and removal mechanisms of advanced ceramics in high speed deep grinding. *International Journal of Machine Tools and Manufacture, 43,* 811–823. https://doi.org/10.1016/S0890-6955(03)00050-6.
11. Ramesh, K., Yeo, S. H., Gowri, S., & Zhou, L. (2001). Experimental evaluation of super high-speed grinding of advanced ceramics. *The International Journal of Advanced Manufacturing Technology, 17,* 87–92. https://doi.org/10.1007/s001700170196.
12. Heard, H. C., & Cline, C. F. (1980). Mechanical behaviour of polycrystalline BeO, Al2O3 and AlN at high pressure. *Journal of Materials Science, 15,* 1889–1897. https://doi.org/10.1007/BF00550614.
13. Huang, H., Damjanac, B., & Detournay, E. (1997). Numerical modeling of normal wedge indentation in rocks with lateral confinement. *International Journal of Rock Mechanics and Mining Sciences, 34,* 613. https://doi.org/10.1016/S1365-1609(97)00169-X.
14. Crossland, B. (1958). The plastic flow and fracture of a 《Brittle》 material (gley cast iron) with particular reference to the effect of fluid pressure. *Proceedings of the Institution of Mechanical Engineers, 172,* 805–820.
15. Yoshino, M., Aoki, T., Sugishima, T., & Shirakashi, T. (1999). Scratching test on hard-brittle materials under high hydrostatic pressure. *Seimitsu Kogaku Kaishi/Japan Society of Precision Engineering, 65,* 1481–1485. https://doi.org/10.1115/1.1347035.
16. Yoshino, M., Aoki, T., Shirakashi, T., & Komanduri, R. (2001). Some experiments on the scratching of silicon: In situ scratching inside an SEM and scratching under high external hydrostatic pressures. *International Journal of Mechanical Sciences, 43,* 335–347. https://doi.org/10.1016/S0020-7403(00)00019-9.
17. Tan, Y., Jiang, S., Yang, D., & Sheng, Y. (2011). Scratching of Al2O3under pre-stressing. *Journal of Materials Processing Technology, 211,* 1217–1223. https://doi.org/10.1016/j.jmatprotec.2011.02.005.
18. Zhang, G., Zeng, Y., Zhang, W., et al. (2016). Monitoring for damage in two-dimensional pre-stress scratching of SiC ceramics. *International Journal of Precision Engineering and Manufacturing, 17,* 1425–1432. https://doi.org/10.1007/s12541-016-0168-8.
19. Zhang, B., Wang, J., Yang, F., & Zhu, Z. (1999). The effect of machine stiffness on grinding of silicon nitride. *International Journal of Machine Tools and Manufacture, 39,* 1263–1283.
20. Lawn, B. R., & Swain, M. V. (1975). Microfracture beneath point indentations in brittle solids. *Journal of Materials Science, 10,* 113–122. https://doi.org/10.1007/BF00541038.
21. Jiang, S., Tan, Y., Zhang, G., et al. (2013). Mechanics model for ceramic materials machining under compressive pre-stress. *Journal of the Chinese Ceramic Society, 6,* 738–744.
22. Conway, J. C., & Kirchner, H. P. (1980). The mechanics of crack initiation and propagation beneath a moving sharp indentor. *Journal of Materials Science, 15,* 2879–2883. https://doi.org/10.1007/BF00550558.
23. Zhou, Yichun. (2008). *Solid mechanics in materials*. China: Beijing.

Gaofeng Zhang Professor in the Engineering Training Center, Xiangtan University in China. His main research interest is the advanced processing technology and tools of hard-to-cut materials.

Zhigang Wang Received M.S. degree in the School of Mechanical Engineering, Xiangtan University in Chian. His research interest is the advanced processing technology of hard-to-cut materials.

Hao Sun Received M.S. degree in the school of Mechanical Engineering, Xiangtan University in Chian. His research interest is the drilling technology of hard-to-cut materials.

Wenxin Chen Received M.S. degree in the School of Mechanical Engineering, Xiangtan University in China. His main research interest is the tribological properties of nano lubrication oil.

KuiZhang in the School of Mechanical Engineering, Xiangtan University in China, received Ph.d degree in the Central South University. His research interest is the design thoery of TBM cutterheads and processing technology of hard-to-cut materials.

Jingtao Li Received M.S. degree in the School of Mechanical Engineering, Xiangtan University in China. His research interest is the morphology reconstruction of grinding wheel and its girnding properties.